ISSN 1063-780X, Plasma Physics Reports, 2020, Vol. 46, No. 5, pp. 496–505. © Pleiades Publishing, Ltd., 2020.
Published in Russian in Fizika Plazmy, 2020, Vol. 46, No. 5, pp. 408–418.

PLASMA TURBULENCE

Anomalous Electron Transport in One-Dimensional Electron Cyclotron Drift Turbulence

A. Smolyakov[a, b, *], T. Zintel[a], L. Couedel[a], D. Sydorenko[a], A. Umnov[b], E. Sorokina[b, c], and N. Marusov[b, c]

[a] *Department of Physics and Engineering Physics, University of Saskatchewan, Saskatoon SK, S7N 5E2 Canada*
[b] *Peoples Friendship University of Russia (RUDN University), Moscow, 117198 Russia*
[c] *NRC "Kurchatov Institute," Moscow, 123182 Russia*
**e-mail: andrei.smolyakov@usask.ca*

Received November 12, 2019; revised December 9, 2019; accepted December 19, 2019

Abstract—The transverse electron current due to the crossed electric and magnetic fields results in the robust instability driven by the electron $\mathbf{E}\times\mathbf{B}$ drift. In the regime of interest for electric propulsion applications, this instability leads to the excitation of quasicoherent nonlinear wave resulting in the anomalous electron transport. We investigate the nonlinear stage of the instability and resulting anomalous electron current using nonlinear Particle-in-Cell simulations. It is found that the anomalous current is proportional to the applied electric field thus demonstrating constant anomalous mobility. Moreover, the scaling of the current density follows the dependence of the dominant resonance wavelength on the electric and magnetic field strength thus clearly demonstrating the cyclotron nature of the instability.

Keywords: cyclotron resonance, plasma accelerators, nonlinear dynamics, particle-in-cell method, anomalous transport, plasma instabilities

DOI: 10.1134/S1063780X20050086

1. INTRODUCTION

The current perpendicular to the confining magnetic field is a source of strong instabilities that have been studied in various applications [1, 2], in particular, in $\mathbf{E}\times\mathbf{B}$ devices for plasma acceleration [3, 4]. The mechanisms of the electron transport in such devices for electric propulsion and similar magnetron systems for material processing are still poorly understood. Recently, this problem has again generated much attention due to interest in new regimes of Hall thrusters [5] and magnetrons [6, 7]. In the fluid limit, the instabilities due to density gradients, $\mathbf{E}\times\mathbf{B}$ drifts and collisions were studied in various conditions [8–16]. Another mechanism exists due to the resonance at the electron cyclotron frequency, ω_{ce}, shifted by the $\mathbf{E}\times\mathbf{B}$ drift, v_E: $\omega - kv_E - m\omega_{ce} = 0$, where ω is the frequency, k is the wave-vector, and m is the number of the resonance). This instability has been studied under different names [2, 17–20]. Here, we adopt the name Electron-Cyclotron-Drift Instability (ECDI) emphasizing the cyclotron resonance features which remain pronounced even in the nonlinear stage. This instability does not require plasma or magnetic field gradients, nor collisions and can be dominant in the regimes of strong electric field. It was studied previously in application to the problem of anomalous resistivity in collisionless shock waves in space and turbulent heating [21–25]. It was also pointed out that this instability can be relevant to $\mathbf{E}\times\mathbf{B}$ Hall accelerators [2, 20].

In the setup relevant to electric propulsion, the ECDI instability is driven by the $\mathbf{E}\times\mathbf{B}$ electron current, so that the unstable waves propagate in the same direction along the $\mathbf{E}\times\mathbf{B}$ electron drift, which is the azimuthal direction of the Hall thruster with the radial magnetic, $\mathbf{B}$, and axial electric, $\mathbf{E}$, fields—see Fig. 1a. The resulting fluctuations of the azimuthal electric field $\tilde{E}_\theta$ produce the axial displacement of electrons and the net axial anomalous current. In geometry of a cylindrical magnetron discharge, the magnetic field is in the axial direction, the electric field is radial, so that the $\mathbf{E}\times\mathbf{B}$ as well as the fluctuations of the electric field are azimuthal, and the resulting anomalous transport is in the radial direction—see Fig. 1b. The direction of the anomalous transport due to particle displacements in the fluctuating electric field is not resolved in the 1D2V Particle-in-Cell (PIC) simulations, but this displacement can be tracked and measured thus giving the value of the anomalous transport due to turbulence [5, 26, 27].

The ECDI is related to the ion-sound instability and under certain conditions becomes similar to the

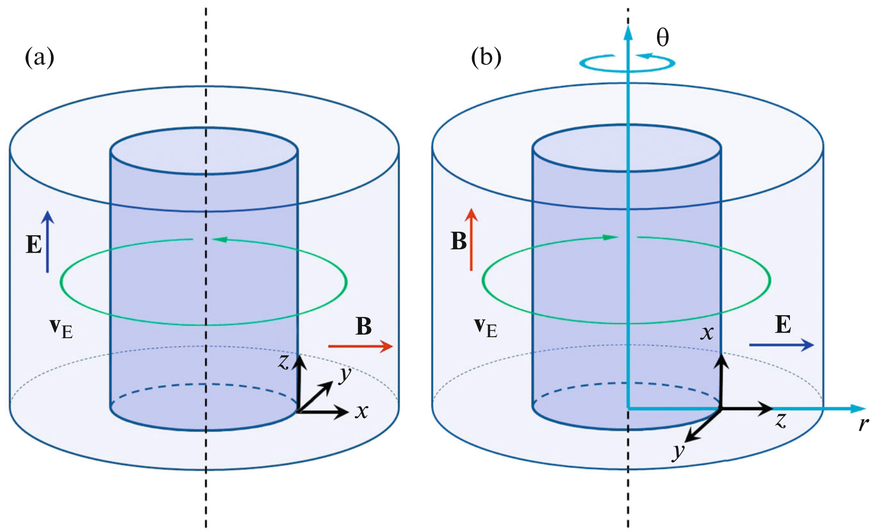

Fig. 1. Configurations of crossed electric and magnetic fields and used coordinate systems in (a) Hall thruster and (b) cylindrical magnetron discharge.

ion sound mode in unmagnetized plasma driven by the relative flow between electron and ion components, so that in some papers it has been called as a modified ion sound instability [2, 28]. A number of recent works [26, 27, 29–31] have interpreted the results of the Particle-in-Cell simulations of the ECDI in regimes relevant to Hall thrusters by using quasilinear expression for the electron transport in the form $\Gamma_z = c\left\langle \tilde{n}\tilde{E}_\theta \right\rangle / B$ (c is the speed of light), while assuming that the phase shift between density, $\tilde{n}$, and electric field fluctuations can be determined as for the unmagnetized ion-sound turbulence in which the only role for the magnetic field is to maintain the electron beam due to the $\mathbf{E}\times\mathbf{B}$ drift. In such theory, the growth rate as in unmagnetized plasma is used with a maximum at the azimuthal wave-vector of the order of the inverse of the electron Debye length, with a full absence of the cyclotron effects.

In our previous work [32] we have found that the assumption of unmagnetized ion-sound turbulence is not applicable for ECDI in typical conditions of the Hall thruster and ECDI retains essential features of the magnetized mode such as the instability drive at the electron cyclotron resonances: the discreet resonances at $\omega - kv_{\rm E} - m\omega_{\rm ce} = 0$ remain clearly pronounced both in the mode growth rate as well as in nonlinear anomalous current. We have also found that the anomalous axial transport is much above the $\Gamma_z = c\left\langle \tilde{n}\tilde{E}_\theta \right\rangle / B$ estimate.

In this paper, we further study the ECDI instability and anomalous transport in one-dimensional nonlinear PIC simulations by incorporating the virtual axial length model. In one-dimensional simulations with externally applied electric $\mathbf{E}_0$ and magnetic $\mathbf{B}_0$ fields, the periodic region along $\mathbf{E}_0\times\mathbf{B}_0$ is resolved. It is the same direction for the induced fluctuations of the electric field $\tilde{\mathbf{E}}$. The latter cause the electron displacement along $\tilde{\mathbf{E}}\times\mathbf{B}_0$, which is the direction of the external electric field $\mathbf{E}_0$. Therefore, anomalous electron transport along the $\mathbf{E}_0$ is accompanied by strong heating due to energy gain from $\mathbf{E}_0$. In one-dimensional simulations with periodic boundary conditions in the azimuthal direction, particles may experience shift along $\mathbf{E}_0$ multiple times resulting in unbound heating in absence of any energy sinks. The virtual axial length model was proposed to circumvent the above problem [5]. In such a model, the net particle displacement in the axial direction is tracked and the particle is removed and replaced with another (cold) particle when the displacement exceeds some length. The choice of the length is dictated by the length of the acceleration region in the Hall thruster, which is of the order of 1–2 cm. This model effectively describes the removal of hot particles from the acceleration region and supply of freshly ionized cold particles instead. With this model, we investigate the features of the ECDI instability and its saturation. One of the goals is to investigate the nature of the instability and presence of resonance (cyclotron) effects. We also study the scaling of the anomalous transport with electric and magnetic fields, and plasma density.

2. LINEAR THEORY OF THE ECDI

Linear theory of the electron-cyclotron drift instability (ECDI) is well described [2, 17]. Here we summarize the linear model in slab geometry to fix the assumptions and our notations. We consider plasma in the crossed electric and magnetic fields, the external electric field $\mathbf{E}_0 = E_0\hat{\mathbf{z}}$ is in the axial direction, while the magnetic field $\mathbf{B}_0 = B_0\hat{\mathbf{x}}$ is in the radial direction of the Hall thruster.

The ions are considered unmagnetized, while the magnetized electrons are subject to the drift in the y-direction (the azimuthal direction): $\mathbf{v}_0 \equiv \mathbf{v}_\mathrm{E} = cE_0/B_0\hat{\mathbf{y}}$. The linear dispersion relation can be presented in the form $1 + \epsilon_\mathrm{i} + \epsilon_\mathrm{e} = 0$, where ϵ_e and ϵ_i are the electron and ion susceptibilities. The response of cold unmagnetized ions is $\epsilon_\mathrm{i} = -\omega_\mathrm{pi}^2/\omega^2$, where ω_pi is the ion plasma frequency. The electron part is

$$\epsilon_\mathrm{e} = \frac{1}{k^2\lambda_\mathrm{D}^2}\left[1 + \frac{\omega - \mathbf{k}\cdot\mathbf{v}_0}{\sqrt{2}k_x v_{T\mathrm{e}}}\sum_{m=-\infty}^{\infty} e^{-b}\mathrm{I}_m(b) \times Z\left(\frac{\omega - \mathbf{k}\cdot\mathbf{v}_0 + m\omega_\mathrm{ce}}{\sqrt{2}k_x v_{T\mathrm{e}}}\right)\right]. \quad (1)$$

Here, $k \equiv |\mathbf{k}| = \sqrt{k_x^2 + k_y^2}$, where k_x and k_y are the components of the wave-vector $\mathbf{k}$ along the magnetic field and in the periodic $\mathbf{E}\times\mathbf{B}$ direction, $b = k^2\rho_\mathrm{e}^2$, $\rho_\mathrm{e}^2 = v_{T\mathrm{e}}^2/\omega_\mathrm{ce}^2$, $v_{T\mathrm{e}}^2 = T_\mathrm{e}/m_\mathrm{e}$, $\lambda_\mathrm{D}^2 = T_\mathrm{e}/(4\pi e^2 n_0)$, T_e is the temperature of electrons, m_e is the mass of electrons, e is the elementary charge, n_0 is the equilibrium plasma density, $Z(\xi)$ is the plasma dispersion function, $I_m(x)$ is the modified Bessel function of the 1st kind.

The solution of the linear dispersion equation (1) was discussed in many papers, e.g., [17, 20, 33, 34]. Here we show the solution from [35], Fig. 2. For small values of the wave-vector along the magnetic field, the growth rate of the instability appears as a set of discreet modes near the resonances $\omega - kv_\mathrm{E} = m\omega_\mathrm{ce}$. In the cold plasma limit, this instability reduces to the reactive Buneman instability [36] as discussed in [35]. Another long wavelength mode occurs for a finite value of k_x along the magnetic field, the so-called modified Buneman two-stream instability (MTSI). However, at the finite electron temperature, when $k_x v_{T\mathrm{e}} > \omega_\mathrm{ce}$, the instability is transformed into the ion sound type mode driven by the inverse Landau damping on the electron $\mathbf{E}\times\mathbf{B}$ beam flow. This is named a modified ion sound instability [2, 28]. The typical picture of the mode growth rate is shown in Fig. 2, where for small values of k_x one has the sharp resonant peaks, and for larger k_x, the resonances overlap resulting in the much slower growth rates described by the unmagnetized dispersion relation which predicts the continuous growth rate with a maximum $\gamma_\mathrm{m} = \omega_\mathrm{pi}\sqrt{\pi/54}v_\mathrm{E}/v_{T\mathrm{e}}$, at $k_y = k_\mathrm{m} = 1/\sqrt{2}\lambda_\mathrm{D}$ with the real part of the frequency $\omega_\mathrm{m} = \omega_\mathrm{pi}/\sqrt{3}$ in the ion frame [27, 37]. In this limit, no effects of the cyclotron resonances are present. The overlap of resonances may also occur due to nonlinear effects and collisions. The question whether the instability indeed becomes of the ion-sound type as in the unmagnetized plasma, or persists as a cyclotron driven mode, remains a long standing problem [18, 38, 39] in the theory of current driven turbulence in the magnetic field.

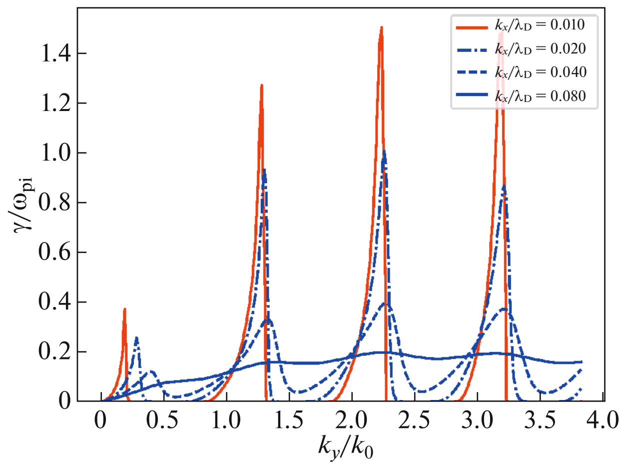

Fig. 2. The linear growth rate of the ECDI, from Eq. (1), for various values of the wave-vector along the magnetic field. The regime of unmagnetized ion-sound instability corresponds to $k_x\lambda_\mathrm{D} = 0.08$. Reprinted with permission from [35].

3. ECDI INSTABILITY AND ANOMALOUS ELECTRON CURRENT IN NONLINEAR PARTICLE-IN-CELL SIMULATIONS

As noted above and illustrated in Fig. 2, in the linear theory, for a sufficiently large value of the wave-vector along the magnetic field, the ECDI instability becomes similar to the ion sound mode in unmagnetized plasma. The collisions can also result in the overlapping and smoothing out the cyclotron resonances, effectively forcing the instability into the ion-sound regime if the electron–neutral collision frequency ν, or the effective frequency due to numerical noise, is sufficiently high $(\nu/\omega_\mathrm{ce})k^2\rho_\mathrm{e}^2 > \pi/2$. Nonlinear resonance broadening [40] can have similar effect for sufficiently large amplitude of fluctuations: $(\omega_\mathrm{pe}^2/\omega_\mathrm{ce}^2)\tilde{E}^2/(8\pi n_0 T_\mathrm{e}) > (k\rho_\mathrm{e})^{-1}$ [32], where ω_pe is the electron plasma frequency. It remains unclear whether any of these mechanisms are fully effective and allow transition of the instability into the unmagnetized regime so that the effects of the magnetic field can be neglected in the nonlinear saturated state for parameters of interest for Hall thruster applications.

The differences between the ion sound type turbulence in unmagnetized plasma and in a plasma with magnetic field were much debated previously in various conditions with many examples that show that even weak magnetic field, $\omega_\mathrm{ce} < \omega_\mathrm{pe}$, strongly affects the turbulence [38, 39, 41, 42]. We note that many PIC simulations relevant to Hall thruster conditions were performed in 1D (azimuthal) and 2D (azimuthal-axial) geometry, when the direction along the magnetic field was not included, $k_x = 0$, and therefore the linear transition to the ion sound regime was not possible, and the only mechanism for smoothing out of cyclotron resonances would be the nonlinear broadening.

In our previous one-dimensional simulations, in nonlinear stage, it was determined that the nonlinear broadening was not effective and the mode essentially remained in the cyclotron resonance regime resulting in a relatively coherent quasi-periodic nonlinear wave. It was also demonstrated that there is the inverse cascade tendency toward formation of large scale modes at the length scale of the simulation box [35]. The total anomalous current was found to be much larger than the $\mathbf{E}\times\mathbf{B}$ quasilinear estimate $\Gamma_z = c\langle \tilde{n}\tilde{E}_y\rangle/B_0$. These simulations however have to be limited to relatively short runs of 1–2 μs due to unbound electron temperature increase, so no true stationary state was achieved.

In this paper, we employ the virtual axial length model that provides effective cooling of electrons and thus allows to reach nonlinear saturation of the electron temperature. With this model, we have performed a series of one-dimensional simulations of ECDI for the magnetic field and electric field typical of the acceleration region for Hall thrusters. The goal of these simulations is to investigate the parametric dependencies of the mode characteristics in the nonlinear saturation state, such as wavelength and anomalous current as a function of the electric and magnetic fields, and plasma density. We have used the implicit PIC code [43, 44]. This code employs widely used Particle-in-Cell methodology to solve kinetic equations for ions and electrons in a self-consistent electric field. The electric field is solved on the fixed grid, while particles are followed on Lagrangian trajectories, and the kinetic equations are solved by method of characteristics. The particles charges are interpolated to the grid, and the electric field is mapped back to the Lagrangian particles position. This techniques is well described [45–47], and details of the particular implementation in the EDIPIC are given in [43]. EDIPIC is an open source code used by several groups in the world and is available from [44]. The code is electrostatic and includes particle collisions, however for the simulations in this paper, the collisions were turned off. The code has been thoroughly tested for various applications [48], and its most recent 2D version was benchmarked by several groups for $\mathbf{E}\times\mathbf{B}$ driven instability [49].

We have performed simulations for several values of the magnetic field $B = 200$, 100, and 400 G, the electric field $E = 5$, 10, 20, and 40 kV/m, and plasma density $n_0 = 10^{17}$, 2×10^{17}, and 0.5×10^{17} m^{-3}. An azimuthal segment of the length $l_y = 26.7$ mm (along the $\mathbf{E}\times\mathbf{B}$ direction) with periodic boundary conditions was considered. The plasma was initialized with an initial temperature $T_e = 10$ eV, the ion atomic weight was 130. The virtual axial length was $l_z = 10$ mm corresponding to the typical length of the acceleration region in the Hall thruster. The energy of the electrons that travelled this distance was changed by a random choice from the $T_e = 10$ eV Maxwellian distribution; the positions of the electrons were not changed. Another method was also suggested [26] where "new" electrons were similarly randomly cooled down but their positions were also randomized along the azimuthal direction. This process becomes equivalent to strong collisions and therefore would introduce too much distortion in the anomalous transport which is of our main interest here. Therefore we have not used it here.

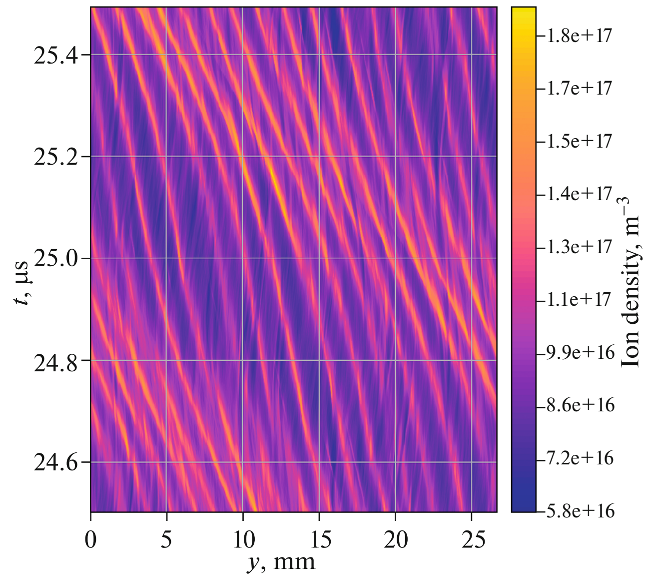

Fig. 3. Propagating ion density perturbations around t_{ce} = 25 μs, for the base case plasma parameters: $B = 200$ G, $E =$ 20 kV/m, and $n = 10^{17}$ m^{-3}. One can see the large-scale mode superimposed with the small-scale quasi-coherent mode.

The current version of the EDPIC [44] with an updated random number generator was used for all runs. All runs were performed on the same cluster (Plato at the University of Saskatchewan) to avoid cross-cluster variations. The spatial grid size was selected to have 3 points within the Debye length at $T_e = 10$ eV. The upper limit for the electron velocity was selected to $12v_{Te}$ corresponding to the CLF validity up to the electron temperature of 1440 eV. The number of particles per cell was MPC = 1241. Simulation results are shown in Figs. 3–9.

The typical behavior of the ECDI in nonlinear regime is similar to what has been observed in [32], and also recently confirmed in [50]: the instability is

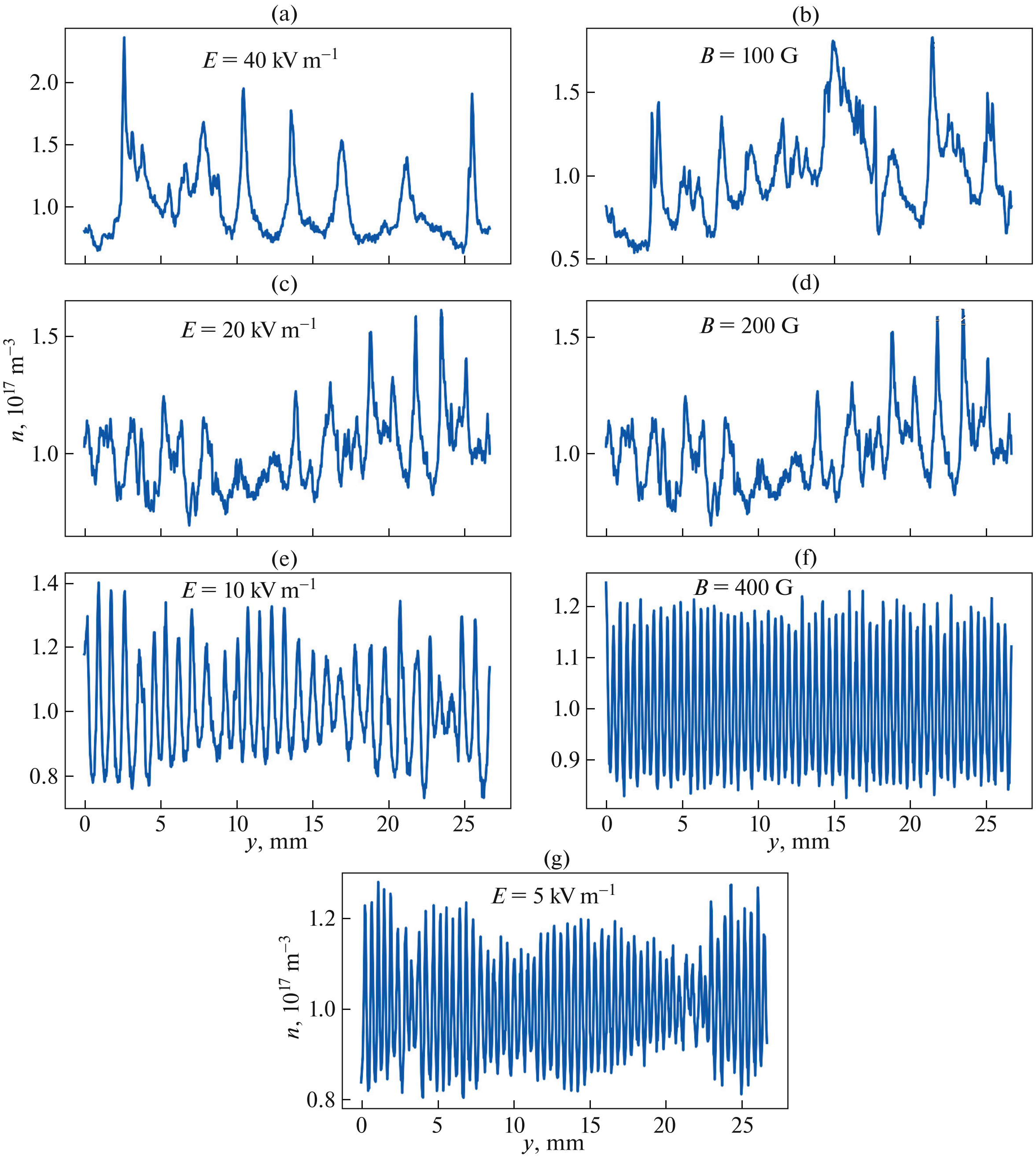

Fig. 4. Spatial variation of the ion density for different values of the electric and magnetic field at 10 μs. The cases with varied electric field are for $B = 200$ G, and the cases with varied magnetic field, are for $E = 20$ kV/m.

dominated by the $m = 1$ resonance. This wavelength, corresponding to the condition $k_y v_E \simeq \omega_{ce}$, appears as a quasicoherent mode shown in Fig. 3. It is worth noting that in the linear theory higher m modes can have the larger growth rates and typically start grow first [32, 35]. However with the increase of the electron temperature and nonlinear inverse cascade the $m = 1$ becomes dominant in the nonlinear stage. The large scale structures, at the length scale of the simulation box, also appear similarly to [32], as evident in Figs. 3 and 4, as well in Fourier spectra, Fig. 5. The dominant Fourier modes are marked by vertical lines in Fig. 5, for corresponding values of the electric and magnetic fields. The time averaged of these values are shown in Figs. 8 and 9 as dominant wavelengths.

For the calculation of long time averaged quantities such as the anomalous current, we chose the range between 10 and 25 μs shown in Fig. 6, in which the current and electron temperature are reasonably in

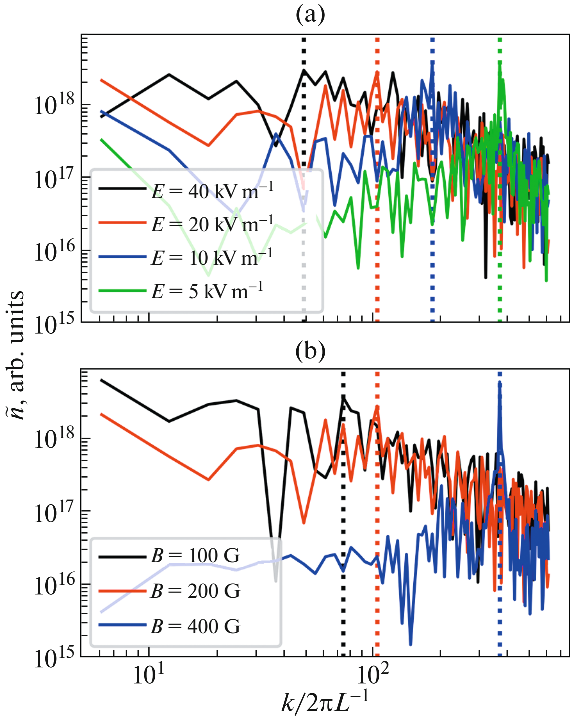

Fig. 5. The spatial Fourier spectra of density fluctuations (in arbitrary units) for the snapshot shown in Fig. 4. The vertical dashed lines mark the wavelength of the maximum amplitude for this case. The averages of these wavelengths (over the 10–25 μs time interval) are shown in Figs. 8c, 8d, and 9b.

stationary state. The time evolution of the electron thermal energy and anomalous current are shown in Fig. 6 for the base case parameters. In these figures, a low pass filtered (1 μs) was applied to show the average current, however the long time averaged data, as shown in Figs. 8 and 9, were calculated from raw data without any filters.

The ECDI instability provides an effective mechanism of the electron heating. As noted above the electrons are initially loaded and further replaced with the temperature of $T_e = 10$ eV. The electrons are heated in turbulent azimuthal oscillations of the electric field as well as due to the anomalous displacement in the direction along the equilibrium electric field. As follows from Figs. 6a, 8g, 8h, the electron temperature saturates (for the base case) around 70 eV, which is higher than the typical values in the Hall thrusters where sheath boundary and two-dimensional energy losses (absent in our model) are important. The electron temperature is isotropic in the plane perpendicular to the magnetic field, due to the effective mixing by the magnetic field. As a matter of fact, the electron distribution function deviates from Maxwellian [32], so the values shown in Figs. 6 and 8 are for the particle kinetic energy.

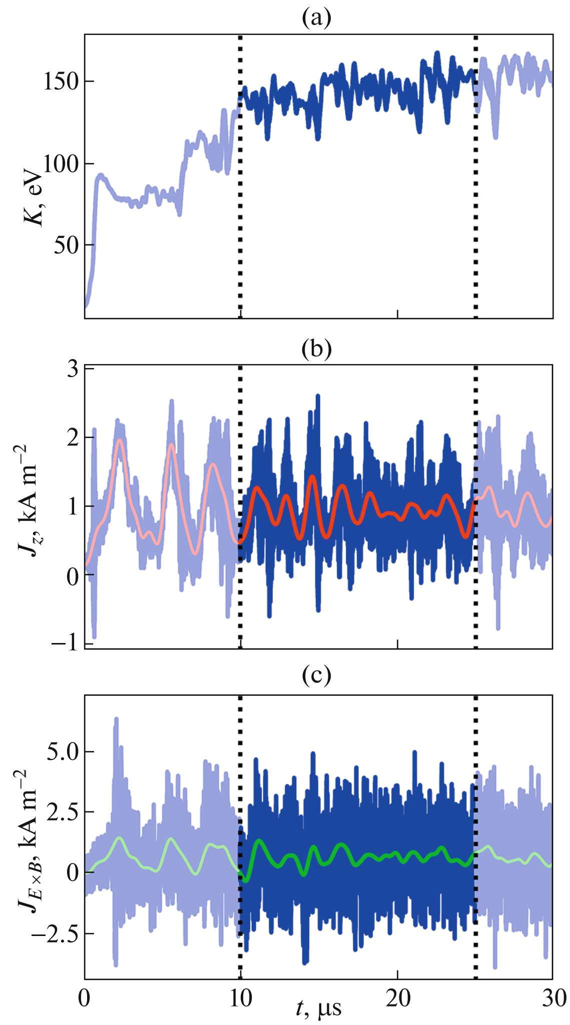

Fig. 6. The time evolution of (a) the total thermal energy of electrons; (b) the net axial current J_z, and (c) the $J_{E\times B}$ current as a function of time for the base case parameters. The raw and low pass filtered ($\delta t = 1$ μs) data are shown. The vertical dashed lines show the time range used for calculation of the average current and energy reported in Figs. 8 and 9.

The anomalous current in our simulations is calculated directly from the electron distribution function as $J_z = -e\int v_z f d^2 v$ and averaged over the azimuthal direction. We also calculate the quantity $J_{E\times B} = ce\langle \tilde{n}\tilde{E}_y/B_0\rangle$ by averaging the fluctuations of the electron density and axial electron drift due to fluctuations of the azimuthal electric field. The difference between the real current J_z and $J_{E\times B}$ allows us to evaluate the degree of the electron "magnetization." The electron velocity is expected to be close to the drift velocity $\mathbf{v}_E = c\mathbf{E}\times\mathbf{B}/B^2$ when the electron Larmor radius ρ_e is much smaller than the fluctuations wavelength $\rho_e \ll \lambda$, and the characteristic frequency is well below

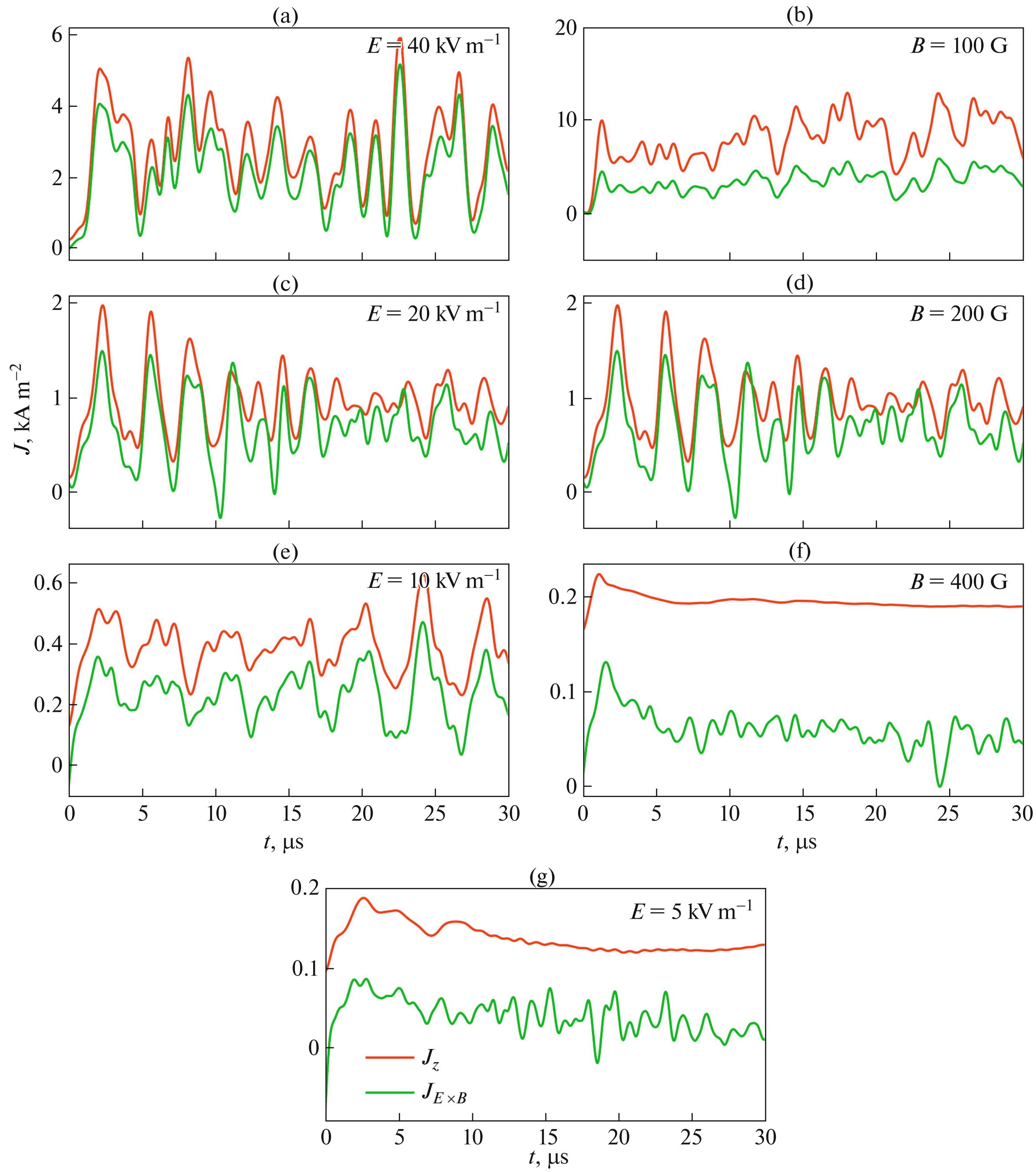

Fig. 7. The low pass filtered ($\delta t = 1$ μs) data of the axial current $J_z = -e\int v_z f d^2 v$ and the $\mathbf{E}\times\mathbf{B}$-current: $J_{E\times B} = ce\langle \tilde{n}\tilde{E}_y/B_0\rangle$ for different values of the electric and magnetic fields. The difference between the J_z and $J_{E\times B}$ becomes significant for higher magnetic field and lower electric field, consistent with the scaling of the dominant wavelength $\lambda \sim E/B^2$: the electron demagnetization is increases for shorter wavelengths.

the electron cyclotron frequency, $\omega \ll \omega_{ce}$. When these conditions are not met, the electrons become "demagnetized" and their velocity is different from $\mathbf{v}_E = c\mathbf{E}\times\mathbf{B}/B^2$. We note that for the base case plasma parameters, $T_e \simeq 70$ eV, $B = 200$ G, $E = 20$ kV/m, the electron Larmor radius, which is of the order of $\rho_e \simeq$ 1 mm, is somewhat smaller than the mode wavelength, which is of the order of 2 mm at these parameters—see Fig. 8c. As Fig. 7 illustrates, the electrons are getting "demagnetized" and the difference between J_z and $J_{E\times B}$ increases for stronger magnetic field and smaller values of the electric field because the dominant mode wavelength becomes comparable

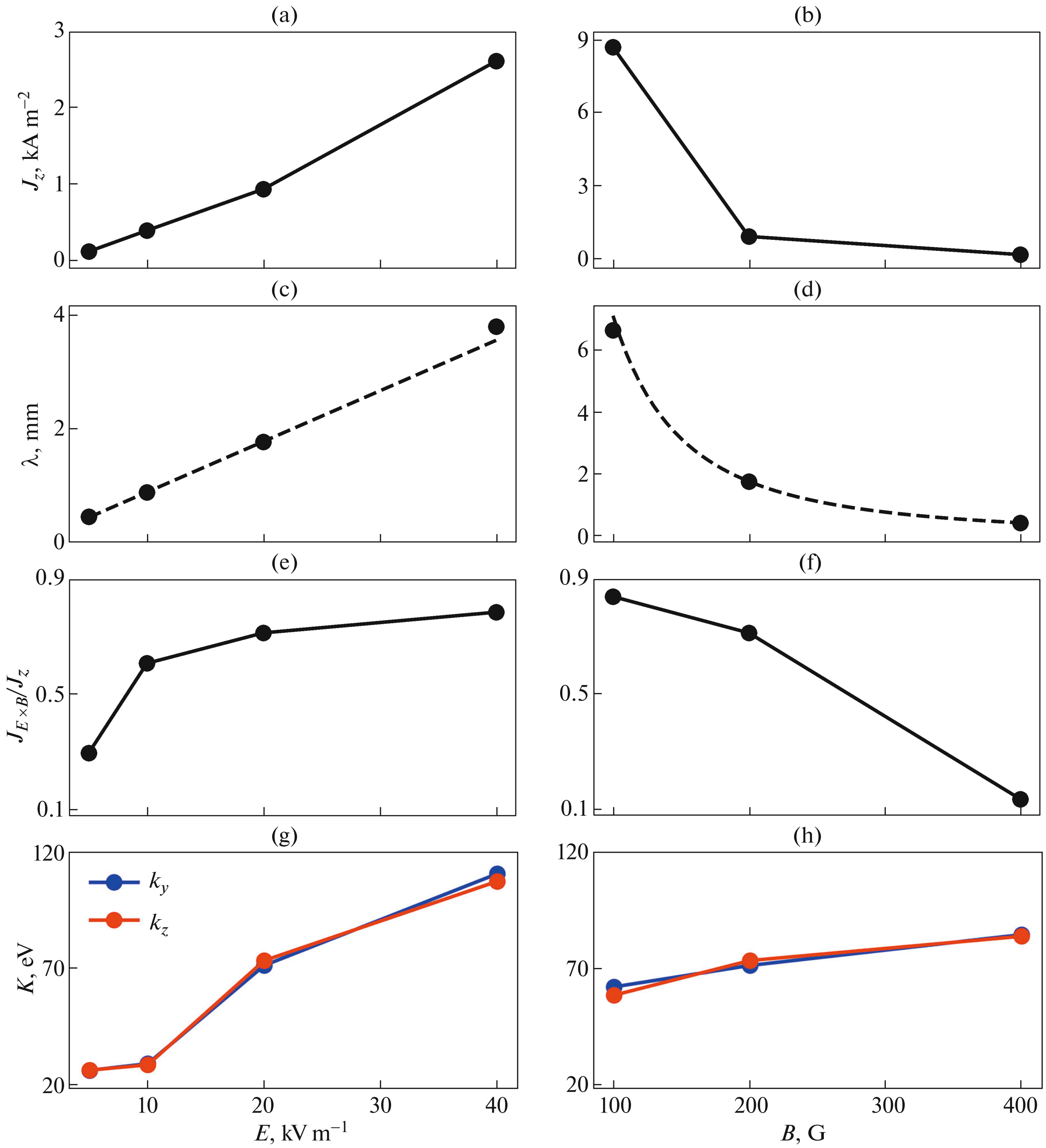

Fig. 8. (a, b) The scaling of the anomalous current, (c, d) the wavelength of the dominant mode, (e, f) the ratio of the $J_{E\times B}/J_z$, and (g, h) electron temperature are shown as function of (a, c, e, g) the electric and (b, d, f, h) the magnetic fields. The dashed lines in (c, d) show the curve $\lambda = 2\pi v_E/\omega_{ce}$.

with the electron Larmor radius, consistent with the scalings $\rho_e \sim 1/B$ and $\lambda \sim E/B^2$—see also the ratio of $J_z/J_{E\times B}$ shown in Figs. 8e, 8f. Varying the magnitude of the electric and magnetic field we demonstrate that the dominate wavelength (averaged over 10–25 μs) is in almost perfect agreement with the expression $\lambda = 2\pi v_E/\omega_{ce}$, as shown Figs. 8c, 8d. No dependency of the wavelength on plasma density, which would be expected for the ion sound wave, is observed in our simulations—see Fig. 9b. Similar result was also reported in [50].

In our simulations, we do observe the formation of the long wavelength (box-size) structures, as is evident in Fig. 3 as well as in the spectra in Fig. 5: note the energy accumulation in the $k \simeq 2\pi/L$ region. Since in our model we do not have a proper dissipation mechanism for large scale structures (no energy sink at the

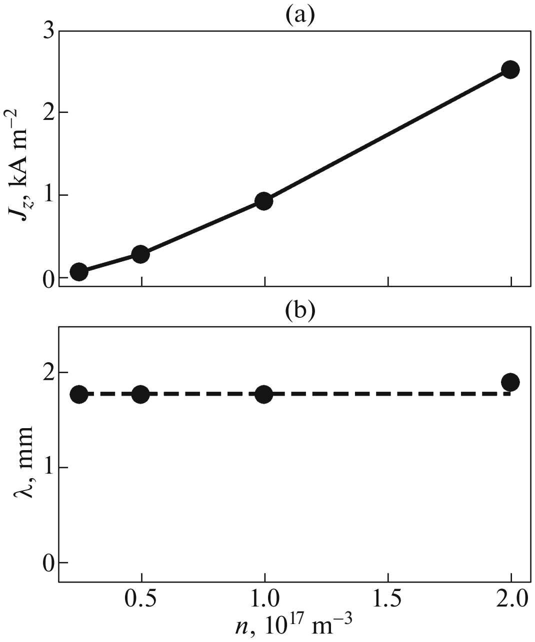

Fig. 9. The scaling of the anomalous current and the wavelength of the dominant mode as a function of plasma density.

box size length scale), we do not expect that large scale structures will reach a stationary state, but rather complex intermittence of large scale and small scale fluctuations is expected. The complex problem of intermittency and dynamics of large scale structures is not considered in our paper. Therefore, we limit the simulations to the time before the long wavelength structures start to dominate the turbulence. For longer simulations, we have observed sudden transitions into the state where a single long wavelength mode becomes dominant; typically such a transition is accompanied by large increase in anomalous current. Such regimes are not considered here.

The scaling of the anomalous current with the electric and magnetic fields is one of the most important result of our study. The anomalous current shown in Fig. 8a shows consistent linear scaling with the constant anomalous mobility, $J_z = \sigma^{an} E_z$. Another result, shown in Fig. 8b, is the inverse dependence of the current with square of the magnetic field, which therefore follows the wavelength scaling, $J_z \sim \lambda \sim 1/B^2$. The latter scaling can also be seen in Figs. 8c, 8d, thus demonstrating that long wavelength modes provides larger anomalous transport. The current density shows the expected linear scaling with plasma density, Fig. 9a. It is also important that the dominant wavelength is independent of plasma density, as shown in Fig. 9b, contrary to the expectation for unmagnetized ion-sound turbulence, where the most unstable mode has a wavelength scaling with the Debye length [26, 27, 37].

4. SUMMARY

A series of one-dimensional simulations of nonlinear ECDI were performed to study the saturation of the instability and the scaling of the resulting anomalous electron current with plasma parameters. Here we have used a virtual axial length model which allows to properly include the finite particle residence time in the acceleration region. Our simulations confirm the quasi-coherent nature of the instability in the nonlinear stage, with the dominant nonlinear wave length determined by the $m = 1$ resonance, $\omega \ll k_y v_E \simeq \omega_{ce}$. Similar to our previous results [32] we also observe nonlinear generation of long wavelength modes via the mechanism similar to the modulational instability [51]. An interesting, and somewhat unexpected result, is the linear scaling of the anomalous current with the electric field thus demonstrating a constant anomalous mobility (independent of the electric field). Variation of the electric and magnetic fields show that the anomalous current scaling follows the behavior of the dominant wavelength. These results clearly demonstrate the cyclotron nature of the instability contrary to the assumption of unmagnetized ion-sound turbulence assumed in a number of previous works.

FUNDING

This work was supported in part by the Russian Science Foundation, project no. 17-12-01470.

REFERENCES

1. V. I. Arefev, A. V. Gordeev, and L. I. Rudakov, in *Proceedings of the 3rd International Conference on Plasma Physics and Controlled Nuclear Fusion Research, Novosibirsk, 1968* (IAEA, Vienna, 1969), p. 143.
2. V. I. Arefev, Sov. Phys. Tech. Phys. **14**, 1487 (1970).
3. A. I. Morozov, Plasma Phys. Rep. **29**, 235 (2003).
4. V. I. Arefev and K. P. Kirdyashev, Sov. Phys. Tech. Phys. **20**, 330 (1975).
5. J. P. Boeuf, J. Appl. Phys. **121**, 011101 (2017).
6. A. Hecimovic, J. Phys. D: Appl. Phys. **49**, 18LT01 (2016).
7. A. Hecimovic, V. Schulz-von der Gathen, M. Böke, A. von Keudell, and J. Winter, Plasma Sources Sci. Technol. **24**, 045005 (2015).
8. Y. V. Esipchuk and G. N. Tilinin, Sov. Phys. Tech. Phys. **21**, 417 (1976).
9. V. Nikitin, D. Tomilin, A. Lovtsov, and A. Tarasov, EPL **117**, 45001 (2017).
10. A. I. Smolyakov, O. Chapurin, W. Frias, O. Koshkarov, I. Romadanov, T. Tang, M. Umansky, Y. Raitses, I. D. Kaganovich, and V. P. Lakhin, Plasma Phys. Control. Fusion, **59** 014041 (2017).
11. D. Tomilin, Phys. Plasmas **20**, 042103 (2013).

12. V. P. Lakhin, V. I. Ilgisonis, A. I. Smolyakov, E. A. Sorokina, and N. A. Marusov, Phys. Plasmas **25**, 012107 (2018).
13. V. P. Lakhin, V. I. Ilgisonis, A. I. Smolyakov, E. A. Sorokina, and N. A. Marusov, Phys. Plasmas **25**, 012106 (2018).
14. N. A. Marusov, E. A. Sorokina, V. P. Lakhin, V. I. Ilgisonis, and A. I. Smolyakov, Plasma Sources Sci. Technol. **28**, 015002 (2019).
15. A. A. Litvak and N. J. Fisch, Phys. Plasmas **8**, 648 (2001).
16. S. Chable and F. Rogier, Phys. Plasmas **12**, 033504 (2005).
17. S. P. Gary, Plasma Phys. Control. Fusion **15**, 399 (1973).
18. M. Lampe, W.M. Manheimer, J. B. McBride, and J. H. Orens, Phys. Fluids **15**, 2356 (1972).
19. D. W. Forslund, R. L. Morse, and C. W. Nielson, Phys. Rev. Lett. **25**, 1266 (1970).
20. J. C. Adam, A. Heron, and G. Laval, Phys. Plasmas **11**, 295 (2004).
21. S. P. Gary and D. Biskamp, J. Phys. A: Gen. Phys. **4**, L27 (1971).
22. D. Forslund, C. Nielson, R. Morse, and J. Fu, Phys. Fluids **15**, 1303 (1972).
23. M. Lampe, J. B. McBride, W. M. Manheimer, R. N. Sudan, R. Shanny, J. H. Orens, and K. Papadopolous, Phys. Fluids **15**, 662 (1972).
24. D. Biskamp and R. Chodura, Phys. Fluids **16**, 893 (1973).
25. A. A. Galeev and R. Z. Sagdeev, in *Handbook of Plasma Physics: Supplement to Basic Plasma Physics*, Vol. 2, Ed. by A. A. Galeev and R. N. Sudan (North-Holland, Amsterdam, 1984), p. 272.
26. T. Lafleur, S. D. Baalrud, and P. Chabert, Phys. Plasmas **23**, 053502 (2016).
27. T. Lafleur, S. D. Baalrud, and P. Chabert, Phys. Plasmas **23**, 053503 (2016).
28. P. J. Barrett, R. J. Taylor, J. M. Sellen, B. D. Fried, and C. F. Kennel, Phys. Rev. Lett. **28**, 337 (1972).
29. I. Katz, I. G. Mikellides, R. R. Hofer, and A. Lopez Ortega, in *Proceedings of the 34th International Electric Propulsion Conference, Kobe, 2015,* Paper IEPC-2015-402.
30. I. Katz, A. Lopez Ortega, B. Jorns, and I. G. Mikellides, AIAA Propulsion and Energy Forum, AIAA 2016-4534 (2016). https://doi.org/10.2514/6.2016-4534
31. T. Lafleur, S. D. Baalrud, and P. Chabert, Plasma Sources Sci. Technol. **26**, 024008 (2017).
32. S. Janhunen, A. Smolyakov, O. Chapurin, D. Sydorenko, I. Kaganovich, and Y. Raitses, Phys. Plasmas **25**, 011608 (2018).
33. A. Ducrocq, J. C. Adam, A. Heron, and G. Laval, Phys. Plasmas **13**, 102111 (2006).
34. J. Cavalier, N. Lemoine, G. Bonhomme, S. Tsikata, C. Honore, and D. Gresillon, Phys. Plasmas **20**, 082107 (2013).
35. S. Janhunen, A. Smolyakov, D. Sydorenko, M. Jimenez, I. Kaganovich, and Y. Raitses, Phys. Plasmas **25**, 082308 (2018).
36. O. Buneman, J. Nucl. Energy, Part C **4**, 111 (1962).
37. J. P. Boeuf and L. Garrigues, Phys. Plasmas **25**, 061204 (2018).
38. D. W. Forslund, R. L. Morse, and C. W. Nielson, Phys. Fluids **15**, 2363 (1972).
39. E. L. Lindman, J. Stat. Phys. **39**, 769 (1985).
40. C. T. Dum and R. N. Sudan, Phys. Rev. Lett. **23**, 1149 (1969).
41. L. Muschietti and B. Lembege, J. Geophys. Res.: Space Phys. **118**, 2267 (2013).
42. D. Biskamp and R. Chodura, in *Proceedings of the 4th International Conference on Plasma Physics and Controlled Nuclear Fusion Research, Madison, 1971,* (IAEA, Vienna, 1972), Vol. 2, p. 265. https://library.psfc.mit.edu/catalog/online_pubs/conference%20proceedings/fusion%20energy%20conferences/1971%20v2%20%20STIPUB288_VOL2.pdf.
43. D. Y. Sydorenko, PhD thesis (University of Saskatchewan, Saskatchewan, 2006).
44. EDIPIC 1D3V Particle In A Cell Code. https://bitbucket.org/sjanhune/edipic/wiki/home.
45. C. K. Birdsall and A. B. Langdon, *Plasma Physics via Computer Simulation* (Taylor & Francis, New York, 2005).
46. A. A. Balmashnov, S. P. Stepina, A. M. Umnov, and M. J. Jimenez, Prikl. Fiz., No. 2, 61 (2016).
47. V. V. Andreev, D. V. Chuprov, V. I. Ilgisonis, A. A. Novitsky, and A. M. Umnov, Phys. Plasmas **24**, 093518 (2017).
48. D. Sydorenko, A. Smolyakov, I. Kaganovich, and Y. Raitses, Phys. Plasmas **13**, 014501 (2006).
49. T. Charoy, J. P. Boeuf, A. Bourdon, J. A. Carlsson, P. Chabert, B. Cuenot, D. Eremin, L. Garrigues, K. Hara, I. D. Kaganovich, A. T. Powis, A. Smolyakov, D. Sydorenko, A. Tavant, O. Vermorel, et al., Plasma Sources Sci. Technol. **28**, 105010 (2019).
50. Z. Asadi, F. Taccogna, and M. Sharifian, Front. Phys. **7**, 140 (2019). https://doi.org/10.3389/fphy.2019.00140
51. V. P. Lakhin, V. I. Ilgisonis, A. I. Smolyakov, and E. A. Sorokina, Phys. Plasmas **23**, 102304 (2016).